Oblique-incidence reflectivity difference microscope for label-free high-throughput detection of biochemical reactions in a microarray format

Xiangdong Zhu, James P. Landry, Yung-Shin Sun, Jeff P. Gregg, Kit S. Lam, and Xiaowen Guo

We describe a recently developed oblique-incidence reflectivity difference (OI-RD) microscope, a form of polarization-modulated imaging ellipsometer, for label-free–high-throughput detection of biomolecular reactions on DNA and protein microarrays. We present examples of application of this technique to end-point and real-time investigations of DNA–DNA hybridization, antibody–antigen capture, and protein–small-molecule binding reactions. Compared to a conventional imaging ellipsometer based on the polarizer–compensator–sample–analyzer scheme and under the off-null condition, a polarization-modulated OI-RD microscope is inherently more sensitive by at least 1 order of magnitude to thickness changes on a solid surface. Compared with imaging surface plasmon resonance microscopes based on reflectance change on falling or rising slopes of the surface plasmon resonance, the OI-RD microscope (1) has a comparable sensitivity, (2) is applicable to conventional microscope glass slides, and (3) easily covers a field of view as large as the entire surface of a 1 in. × 3 in. (2.54 cm × 7.62 cm) microscope slide.

OCIS codes: 180.180, 170.170, 310.0310, 240.0240.

1. Introduction

Optical techniques have played an instrumental role at almost every stage of advancement in life sciences. With the advent of lab-on-chips, namely, microarrays of biological macromolecules and individual cells immobilized on solid supports, we are in an exciting era of life sciences when molecular-level and cellular-level chemistry is being explored and characterized in a highly parallel fashion.[1,2] This approach complements conventional molecular and cellular biochemistry approaches. Given the multitude and cooperative aspects of interactions among biological molecular complexes at cellular and subcellular levels, parallel detection of tens or thousands of biochemical reactions in microarray format will accelerate the process of discovery. Fluorescence labeling is commonly used in detection of biochemical reactions in the microarray format.[1,2] Typically one of the reaction partners is tagged with a fluorescent molecule or a quantum dot (through either genetic engineering such as incorporation of green fluorescence protein or a direct reaction with the host molecule). Fluorescence labeling enables the detection of as few as a single macromolecule and drives the field of single-molecule detection in molecular and/or cellular biology.

However, an extrinsic tag such as a fluorescent molecule or a quantum dot always changes the properties of a host macromolecule. The significance of the change is often not known *a priori.* This is particularly relevant when studying properties of proteins.[3] Subtle changes in binding affinities and associated kinetics of protein molecules, by added physical properties of an extrinsic tag or through tag-induced conformational changes in protein molecules, can have a profound influence on some functions of protein molecules. Recognition of stereo-chemically modified double-stranded DNA by specialized proteins in a living system is an example.[4] It is thus sensible to develop label-free detection techniques with adequate sensitivities to complement the fluorescence-based detection methods.

Imaging surface plasmon resonance (SPR) spectroscopy,[5–7] imaging optical ellipsometry (OE),[8–11] and reflectometric interference spectroscopy[12] (RIFS) are

X. D. Zhu (xdzhu@physics.ucdavis.edu), J. P. Landry, and Y. S. Sun are with the Department of Physics, University of California, Davis, Davis, California 95616. J. P. Gregg and K. S. Lam are with the School of Medicine, University of California, Davis, Sacramento, California 95817. X. W. Guo is with the Clinical Diagnostics Group, Bio-Rad Laboratories, 4000 Alfred Nobel Drive, Hercules, California 94547.

Received 29 June 2006; revised 1 September 2006; accepted 15 September 2006; posted 19 September 2006 (Doc. ID 72516); published 13 March 2007.

0003-6935/07/101890-06$15.00/0

some of the optical techniques that have been explored to meet such a need. In their respective ways, these three label-free optical techniques in essence measure the same optical dielectric response of a thin film, consisting of molecules of biological significance on a solid substrate. As a result they detect the same physical or chemical properties of the thin film such as thickness and mass density (including surface coverage) or their changes during biochemical reactions. So far, only imaging SPR and imaging ellipsometry have been explored for high-throughput detection of microarrays of biological molecules.[5–11]

In a SPR microscope equipped with a CCD camera, one typically uses the reflectance of a collimated, monochromatic light at a fixed incidence angle as the contrast and obtains a SPR image of an illuminated area on a solid surface covered with microarrays of biomolecules of interest. To maximize the sensitivity, the incidence angle is chosen to be on the falling or rising slope of the SPR peak. Over 2 orders of magnitude, the reflectance changes linearly with the thickness and the mass density (through the optical dielectric constant or refractive index of the film). The proportionality constant can vary from one gold-coated substrate to another and thus needs to be calibrated if quantitative information is required from such an image. Shumaker-Parry and Campbell[6] were able to quantify the performance of such an imaging SPR microscope and achieved a detection limit of 2×10^{-5} RIU (refractive index unit) or 0.01 nm in detected protein thickness simultaneously over an area of 5 mm $\times$ 5 mm. It remains to be explored how such a microscope may be extended to examine microarrays over a much larger area.

Optical ellipsometry, in one form or another, measures changes in magnitude and phase of complex optical reflectivity (i.e., Fresnel reflection coefficient) in response to changes on solid or liquid surfaces.[8] If one is not concerned with magnetic and chiral properties of a surface layer, relevant reflectivity changes are those for *p*-polarized (transverse magnetic) and *s*-polarized (transverse electric) components of an optical beam. At oblique incidence, in response to a surface-bound change such as a biochemical reaction, the complex reflectivity changes disproportionately for *p*- and *s*-polarized light at a fixed optical frequency. As a result the magnitude and the phase of the ratio of the Fresnel coefficient for *p*-polarized light to that for *s*-polarized light, $r_p/r_s \equiv \rho \equiv \tan\psi \exp(i\delta)$, change. Optical ellipsometry measures such changes.

In a typical imaging ellipsometer, one uses the polarizer–compensator–sample–analyzer (PCSA) scheme in which the phase compensator (C) is fixed and the polarizer (P) and the analyzer (A) are variable. The light beam reflected from an illuminated area on the sample surface (S) passes through the analyzer (A) and is subsequently imaged onto a CCD camera. The P and A are rotated until the photocurrents are more or less minimized across the image region on the CCD to yield ψ and δ maps before, for example, a biochemical reaction takes place on the sample surface. During a subsequent biochemical reaction on the sample surface that results in a thickness change Δd in a surface-bound microarray feature, the corresponding change in the photocurrent under this off-null condition is proportional to $(\Delta\psi)^2$ and $(\Delta\delta)^2$, thus proportional to $(\Delta d/\lambda)^2$. The off-null photocurrents are monitored in real-time to detect the biochemical reactions. However, the quadratic dependence of the off-null photocurrent on already small quantities $\Delta\psi$ and $\Delta\delta$ sets the detection limit of this type of imaging ellipsometer to roughly $\Delta\psi \sim 0.01°$ and $\Delta\delta \sim 0.01°$ (i.e., $\sim$0.0002 rad).

A more sensitive form of ellipsometry is the oblique-incidence reflectivity difference (OI-RD) technique.[6,7] It is a polarization-modulated nulling ellipsometry in which the harmonics of modulated photocurrents are measured under suitable nulling conditions and are *directly* proportional to $\Delta\psi$ and $\Delta\delta$. This makes an imaging ellipsometer based on the measurement of OI-RD signals at least an order of magnitude more sensitive than the aforementioned imaging ellipsometer, namely, with the detection limit to $\Delta\psi \sim 0.001°$ and $\Delta\delta \sim 0.001°$. Such sensitivity is required for high-throughput affinity detection of low molecular weight analytes. The detection limit of $\Delta\delta \sim 0.001°$ corresponds to 0.01 nm in detected protein thickness, similar to that of an imaging SPR microscope.[6]

2. Oblique-Incidence Reflectivity Difference: a Polarization-Modulated Nulling Ellipsometry

Let $r_{p0} = |r_{p0}| \exp(i\Phi_{p0})$ and $r_{s0} = |r_{s0}| \exp(i\Phi_{s0})$ be the reflectivity for *p*- and *s*-polarized light from a bare substrate surface, respectively. Let $r_p = |r_p| \exp(i\Phi_p)$ and $r_s = |r_s| \exp(i\Phi_s)$ be the reflectivity when an ultrathin film is deposited on the substrate or when the surface layer of the substrate is modified. The fractional reflectivity change is defined as $\Delta_p = (r_p - r_{p0})/r_{p0}$ and $\Delta_s = (r_s - r_{s0})/r_{s0}$. The difference in fractional reflectivity change is then $\Delta_p - \Delta_s$. When it is small, $\mathrm{Re}\{\Delta_p - \Delta_s\} = (|r_p| - |r_{p0}|)/|r_{p0}| - (|r_s| - |r_{s0}|)/|r_{s0}|$ is simply the differential magnitude change, $\mathrm{Im}\{\Delta_p - \Delta_s\} = (\Phi_p - \Phi_{p0}) - (\Phi_s - \Phi_{s0})$ is the differential phase change. In terms of $\rho = r_p/r_s = \tan\psi \exp(i\delta)$, $\Delta_p - \Delta_s \approx (\rho - \rho_0)/\rho$ with $\mathrm{Re}\{\Delta_p - \Delta_s\} \approx (\psi - \psi_0)/\sin\psi_0 \cos\psi_0 = \Delta\psi/\sin\psi_0 \cos\psi_0$ and $\mathrm{Im}\{\Delta_p - \Delta_s\} = \delta - \delta_0 = \Delta\delta$.[8] The OI-RD technique has been successfully applied to the detection of a wide variety of ultrathin films and surface modifications ranging from vapor-phase deposited rare gas films and perovskite oxide films in vacuum,[13,14] electrochemically deposited metallic films at liquid–solid interfaces,[15] to microarrays of biological molecules on functionalized glass (i.e., gene chips and protein chips).[11]

To relate the structural information on an ultrathin film or the modified surface layer on a substrate to the experimentally measured $\Delta_p - \Delta_s$, we use a classical three-layer model to describe the optical response from the surface of a homogeneous substrate

covered with an ultrathin film (or a modified surface layer)[16]:

$$\Delta_p - \Delta_s \cong -i\left[\frac{4\pi\varepsilon_s(\tan\theta_{inc})^2\cos\theta_{inc}}{\varepsilon_0^{1/2}(\varepsilon_s-\varepsilon_0)(\varepsilon_s/\varepsilon_0-(\tan\theta_{inc})^2)}\right] \times \frac{(\varepsilon_d-\varepsilon_s)(\varepsilon_d-\varepsilon_0)\Theta}{\varepsilon_d}\left(\frac{d}{\lambda}\right), \quad (1)$$

where θ_{inc} is the incidence angle; ε_0, ε_d, and ε_s are the optical dielectric constants of the ambient, the film (or the modified surface layer), and the substrate, respectively; d is the thickness of the film; and Θ is the coverage of the film on the substrate, i.e., the ratio of the covered area to the total area. Changes other than thickness and coverage such as mass density, chemical make up, and morphology are represented by corresponding changes in ε_d. In addition to the dependence on structural properties of the ultrathin film (d, Θ, and ε_d), $\Delta_p - \Delta_s$ also depends on θ_{inc}. It is maximized when θ_{inc} is close to the Brewster angle θ_B on a transparent substrate or its equivalent on an opaque substrate.[17] From Eq. (1), it is clear that at the interface of two transparent media (ε_0 and ε_s being real), a layer of nonabsorbing biomolecules (ε_d is also real) only leads to a nonzero $\mathrm{Im}\{\Delta_p - \Delta_s\}$. This is what we observe for unlabeled DNA and protein microarrays. It is noteworthy that the SPR technique (another label-free optical detection) measures the same properties (thickness and density) of a surface layer from the shift in the SPR angle, $\delta\theta_{SPR} \approx (3\pi d/\lambda)(\varepsilon_d - \varepsilon_0)/\varepsilon_d$.[18,19] In addition to being as sensitive as the SPR technique when operated near θ_B,[19] the OI-RD technique is applicable to all flat solid substrates and in this respect is more versatile since high-quality metal coatings are not required, and the total internal reflection condition is also not necessary. As a result it is suited for high-throughput detection of microarrays fabricated on conventional solid substrates such as microscope slides. We have developed optical scanning microscopes using $\Delta_p - \Delta_s$ as contrasts and performed a number of proof-of-principle experiments on DNA microarrays and protein microarrays.

3. Applications of Oblique-Incidence Reflectivity Difference Microscopes to Detection of Biomolecular Reactions on Microarrays

The arrangement of an OI-RD microscope is shown in Fig. 1. The procedures for obtaining $\Delta_p - \Delta_s$ have been described in detail by Thomas and co-workers.[13] In this case, the ambient is air with $\varepsilon_0 = 1$, the substrate is glass with $\varepsilon_s = 2.31$. In a microscope configuration, a microarray-covered glass slide is mounted on a dual-axis translation stage underneath fixed illumination and detection optics. The stage is driven by computer-controlled stepper motors and is movable along two perpendicular directions of the glass slide surface.

For *high-resolution imaging*, we focus the illumination beam to a spot of 2.4 μm (the full width at $1/e^2$ of the maximum of the intensity profile) on the microarray-covered surface and image the reflected beam from the spot onto a single photodiode detector. Using Rayleigh's criterion, the image resolution is nominally 1.7 μm. To obtain a 2D image of a microarray using $\Delta_p - \Delta_s$ as contrasts, we mechanically move the stage in both x and y directions and record the values of $\Delta_p - \Delta_s$ at each spot. The scan time is long in this configuration. For high-speed imaging with a spatial resolution of 15 μm to capture both end points and kinetics of biomolecular reactions on 1000-feature or 10,000-feature microarrays (with the feature size in the range of 100 μm and feature separation in the range of 300 μm), we use cylindrical optics to focus the illumination beam into a line on the microarray-covered surface and image the reflected beam from the line onto a multielement photodiode array (instead of a single detector). The scan along the line direction is then achieved by electronically interrogating the elements of the photodiode array at a rate at least 1000 times faster than the mechanical scan. This has enabled us to obtain an end-point image of 800-feature microarrays in less than 14 min as shown in Fig. 2. We should note that in application to microarrays, the spatial resolution in the range of 1.7 to 15 μm is more than enough since typical printed microarray features are between 80 and 150 μm, and typical separation between neighboring features is between 200 and 500 μm.[1] There is no observable edge effect arising from the finite size of the microarray features. In our present OI-RD microscopes, we achieved a sensitivity of 0.1 Å. In terms of resonance unit (RU) routinely used in SPR biosensors, we achieved a sensitivity of 1 RU or 0.0001°. Such sensitivity is adequate for our current microarray applications in small-molecule library screening for protein ligands and in small-molecule drug screening. And it is comparable to SPR microscopy as reported by Shumaker-Parry and Campbell.[6]

In Fig. 3(a), we show an $\mathrm{Im}\{\Delta_p - \Delta_s\}$ image of a 3×3 60-nucleotide (*nt*) oligomer microarray after it has reacted with a mixture of unlabeled 60-*nt* oligomers complementary to column 1 and Cy5-labeled 60-*nt* oligomers complementary to column 3. Each column is a triplicate of 120 μm spots of oligomers with

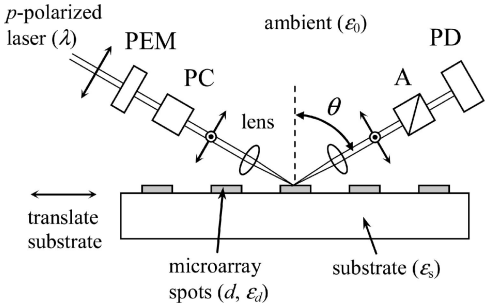

Fig. 1. OI-RD microscope for imaging biomolecular microarrays on a functionalized glass substrate. The substrate is on a translation stage that is movable along the x and y directions. PEM, photoelastic modulator for polarization modulation; PC, Pockel's cell for initial phase-shift adjustment; A, polarizing analyzer; PD, single-element or multielement photodetector.

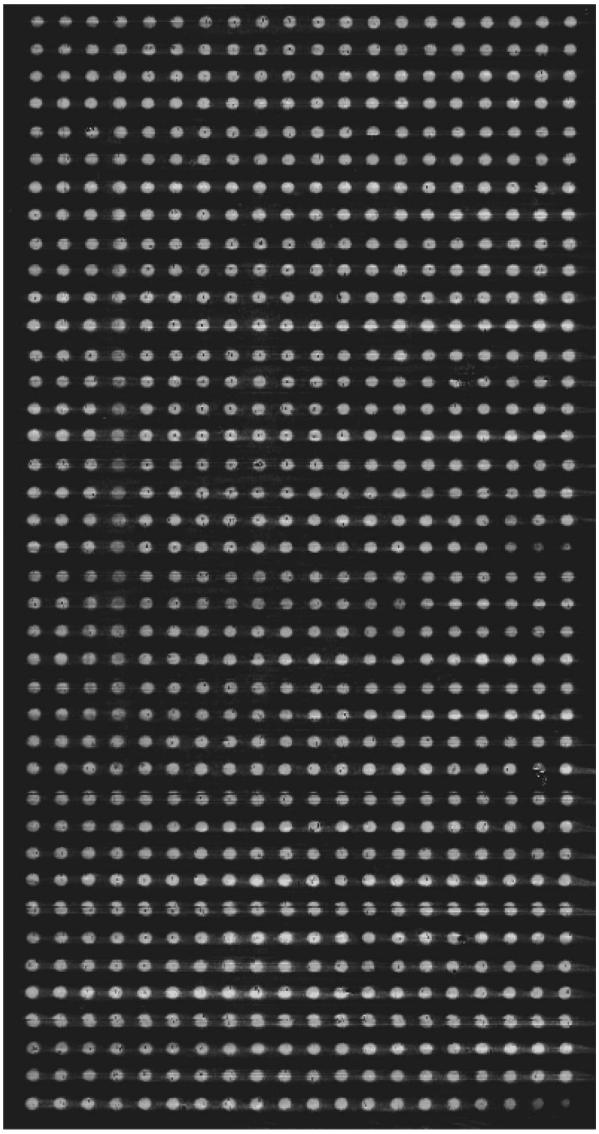

Fig. 2. OI-RD image of a 20 × 40 BSA microarray of one monolayer in thickness, obtained with a high-speed OI-RD microscope using a combination of line illumination and 152-element photodiode array detector. The contrast mechanism is $\mathrm{Im}\{\Delta_p - \Delta_s\}$. The contrast shown in the figure is on average what we have expected of a full BSA monolayer covering each of the 800 features. The pixel dimension of the image is 15 μm × 15 μm. There are 410 × 760 pixels in the image. The feature is 130 μm in diameter, and the center-to-center separation between neighboring features is 300 μm. The total scan time for this 800-feature image is 14 min. The N.A. of this microscope is 0.15.

a well-defined sequence: 5′-TCACAAACCC GTCC TACTCT ACTAGCTGCA GTAGCCCCAC TGGTTC CCGT TTCCGATGTT-3′ for column 1; 5′-CCTTG TACCG CTGAGTTCAC ACCGACACAC CTCACCA CAC TTACACCGTC CACAAAGAGA-3′ for column 2; and 5′-TTTCCATGCG GACCTACCAC CGTAGTA CCT CGCAATGCCA GTGCAACAAG TACACCTG GA-3′ for column 3. The oligomer microarray is printed on a commercial poly-*L*-lysine functionalized glass slide. The printed oligomers lie flat on the glass surface due to the electrostatic interaction between the negatively charged DNA backbone and the positively charged amine group at neutral pH. The excess oligomers on top of the oligomer monolayer are removed by a washing step. The rest of the poly-*L*-lysine functionalized surface is blocked with succinic anhydride in borate-buffered 1-methyl-2-pyrolidinone before the microarray is subjected to the hybridization reaction. The image shown in Fig. 3(a) is the difference between the image taken *after* the reaction and the image taken *before* the reaction. The scale bar is 100 μm in length. The average optical signal change is 1.5×10^{-3} in column 1 and indicates that 60% ($\Theta = 0.6$) of the surface-immobilized oligomers have reacted with complementary partners. The hybridization is well resolved without extrinsic labeling. The average optical signal change in column 3 (the positive control column) is also 1.5×10^{-3}.[6] This is expected since the wavelength of the He–Ne laser used for illumination of the OI-RD microscope is far from the absorption peaks for Cy5 dye.

In Fig. 3(b), we display an $\mathrm{Im}\{\Delta_p - \Delta_s\}$ image of a 4 × 4 protein microarray after it has been exposed to unlabeled goat antibody against rabbit IgG. Each column of the microarray is a titration series in printing concentration (6.7, 5.0, 3.8, and 2.8 μM) of one type of protein: bovine serum albumin (BSA) for column 1; rabbit IgG (RB) for column 2; mouse IgG (MS) for column 3; and human IgG (HM) for column 4. They are printed as 150 μm spots on an epoxy-functionalized glass slide. The excess of the printed proteins is removed by washing steps and the rest of the epoxy-functionalized surface is blocked with BSA. Again, the image shown in Fig. 3(b) is the difference between the one taken after the reaction and the one taken before the reaction. The scale bar is 100 μm. Without fluorescent labeling, the differential image reveals clearly the specific antibody–antigen capture with a good signal-to-noise ratio. The change in $\mathrm{Im}\{\Delta_p - \Delta_s\}$ (4×10^{-3}) indicates that roughly 20% ($\Theta = 0.2$) of a saturated monolayer of RB has reacted with the goat anti-RB.

In Fig. 3(c), we show an $\mathrm{Im}\{\Delta_p - \Delta_s\}$ image of another 3 × 3 protein microarray after it has been exposed to *unlabeled* streptavidin. Each column is a triplicate of 150 μm spots of the same protein: HM for the first column; BSA–biotin complex for the second column; and BSA alone for the third column. The BSA–biotin complex is synthesized for the purpose of "immobilizing" small molecules such as biotin to an epoxy-functionalized glass slide with BSA as the anchor. A linker molecule is inserted between BSA and biotin to minimize the effect of BSA on the affinity of biotin. The image shown in Fig. 3(c) is the difference between the one taken after the reaction and the one taken before the reaction. The specific reaction of streptavidin with BSA–biotin complex is clearly shown in the differential OI-RD image. The bright spots in the images shown in Fig. 3 are dust particles from the ambient and residuals from the processing of the microarray. Streptavidin is roughly a spherical molecule with a 5 nm diameter[20,21] and a mass

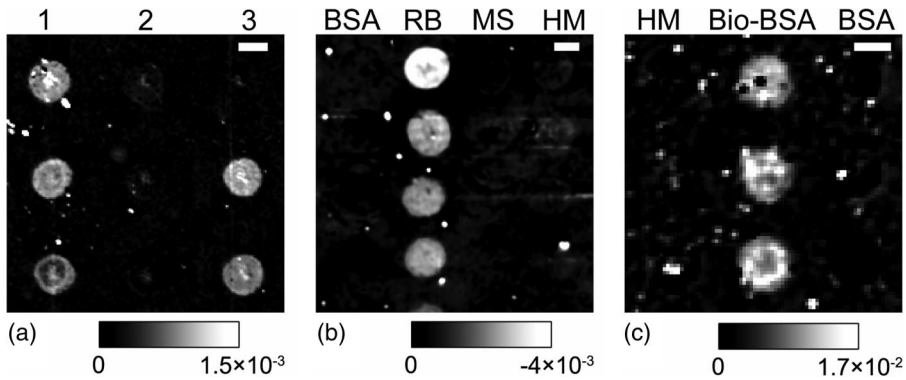

Fig. 3. (a) Image in $\mathrm{Im}\{\Delta_p - \Delta_s\}$ of a 3×3 60-*nt* DNA microarray after reaction with a mixture of unlabeled DNA complementary to the first column and Cy5-labeled DNA complementary to the third column. Incidence angle θ_{inc} is 45°. (b) Image in $\mathrm{Im}\{\Delta_p - \Delta_s\}$ of a 4×4 antigen microarray after reaction with unlabeled goat anti-RB. θ_{inc} is again 45°. (c) Image in $\mathrm{Im}\{\Delta_p - \Delta_s\}$ of a 3×3 protein microarray after reaction with unlabeled streptavidin. θ_{inc} in this case is 59°. The spatial resolution of the microscope that we used to obtain these images is 3 μm.

volume density of $\rho_d = 1.35\ \mathrm{g/cm^3}$. When packed in square lattices to a full monolayer, the surface number density of streptavidin is 4.0×10^{12} molecules/cm^2, and the surface mass density is 4 ng/mm^2. Assume that the optical dielectric constant for streptavidin at $\lambda = 532$ nm is ε_d (streptavidin) = 2.51 [n_d (streptavidin) = 1.584]; we can deduce the surface coverage Θ of the reacted streptavidin using Eq. (1) from the change in the OI-RD signal. After taking into account the effect of the incidence angle at 59°, the change in $\mathrm{Im}\{\Delta_p - \Delta_s\}$ (1.7×10^{-2}) shows that the coverage of the streptavidin is 1.4×10^{12} molecules/cm^2, namely, $\Theta = 0.35$. We should note here that the surface coverage obtained this way is an approximate to the true value as the former depends on the assumption of $\varepsilon_d = 2.51$, the packing geometry, and the validity of Eq. (1). The true relation between the OI-RD signal and the surface coverage can be established in future investigation by a calibration against a fluorescence method or a nuclear method.

To illustrate that the OI-RD technique is capable of measuring protein–small-molecule binding reactions on functionalized glass surfaces in real time, we performed a series of measurements on BSA on an epoxy-coated glass slide. Because of the small dielectric contrast or refractive index difference between glass and water, the reflection from the interface is very weak, making ellipsometry measurements of biomolecular processes at the interface a difficult task. In our experiments, the functionalized side of the glass slide is in contact with the buffer or the BSA solution as part of a fluid cell. The other side of the slide is in air. The illumination laser beam is incident on the functionalized surface through the air side and the reflected beam is detected as illustrated in Fig. 1 with a single detector. The experiment begins with $1 \times$ phosphate buffered saline (PBS) solution in the fluid cell, and then BSA is added and quickly mixed with the $1 \times$ PBS (using a magnetic stir in the cell) to make it a 7.2 μM BSA solution (1.0 mg/ml) in less than 6 s. In Fig. 4 we show $\mathrm{Im}\{\Delta_p - \Delta_s\}$ from the glass–solution interface before and after BSA is added (at $t = 0$) to the $1 \times$ PBS. Except for the first 6 s when the mixture is being homogenized, the OI-RD signal shows the uptake of one monolayer of BSA that fully covers the epoxy-functionalized glass. The saturation level at 0.008 is not changed when the BSA solution is replaced with $1 \times$ PBS, indicating that the uptake or adsorption of BSA is irreversible. This uptake curve compares well with the observation of BSA adsorption from an aqueous buffer on a gold-coated substrate reported by Jung *et al.* using a SPR microscope.[7] By subsequently exposing the BSA-covered glass slide with Cy5-labeled IgG molecules, we were able to confirm that the saturation level at 0.008 in $\mathrm{Im}\{\Delta_p - \Delta_s\}$ corresponds to one full monolayer of BSA that covers 98% of the epoxy-coated surface. From Eq. (1) we find that the signal level of 0.008 corresponds to a uniform layer of BSA with a thickness of 1.4 nm and an effective dielectric con-

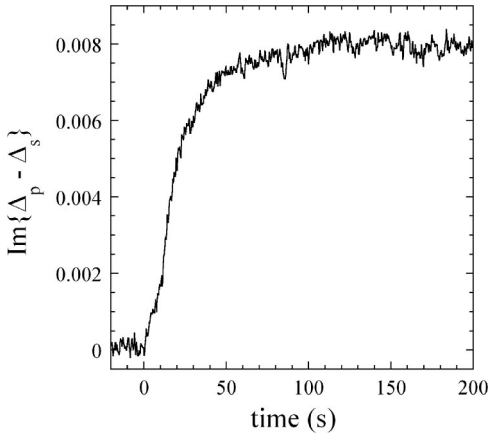

Fig. 4. $\mathrm{Im}\{\Delta_p - \Delta_s\}$ from the interface between an epoxy-functionalized glass slide and the aqueous solution of BSA in $1 \times$ PBS. At $t = 0$, the BSA is added to an initial $1 \times$ PBS to make it a 7.2 μM BSA solution in less than 6 s. The saturated signal level at 0.008 corresponds to a full monolayer of BSA that covers 98% of the epoxy-functionalized surface. A magnetic stir is inside the fluid cell to continuously mix the solution during the experiment, ensuring a constant flux of BSA toward the glass surface.

stant of ε_d (BSA) = 2.5 or a refractive index of n_d (BSA) = 1.58. It is difficult to determine independently the refractive index and the thickness of the BSA layer. By keeping the magnetic stir on during the entire experiment, we maintain a constant BSA flux toward the glass surface (namely, 6 s after the BSA is added.) Figure 4 shows that the uptake follows the Langmuir kinetics, namely, (a) the uptake rate is proportional to the probability of an impinging BSA to strike an open epoxy-coated surface, and (b) the probability of a striking BSA molecule to bind to the open epoxy-coated surface is a constant.

The result shown in Fig. 4 demonstrates that even with a small dielectric contrast between a glass slide and an aqueous solution, the biochemical reaction at the interface can be captured in real time with good sensitivity using the OI-RD technique. By employing a multielement array detector such as the one used to obtain the image in Fig. 2, we can further remove the effect of systemic changes in an OI-RD microscope and in a fluid cell on the measured signal and achieve an even better sensitivity than that displayed in Fig. 4. More importantly, we can simultaneously measure multiple biochemical reactions on a microarray with a high-speed OI-RD microscope.

4. Conclusion

We demonstrated that the oblique-incidence reflectivity difference (OI-RD) as a special form of polarization modulated ellipsometry is a most sensitive, versatile optical platform for label-free detection of biomolecular reactions, particularly in microarray format. In microscope configurations, this ellipsometric technique is suited for very-high-throughput screening of small molecule libraries for protein ligand candidates and for high-throughput search for biomarkers. Because an OI-RD microscope is capable of both end-point and real-time measurements in a highly parallel fashion, we expect it to be instrumental in discovery-oriented and function-oriented proteomic research from molecular to cellular levels.

This work was supported by the Graduate Research and Education in Adaptive Biotechnology (GREAT) program under grant 2004-09, administered by the University of California Systemwide Biotechnology Research and Education Program, by the NSF Center for Biophotonics Science and Technology, and by the National Institutes of Health under NIH-R01-HG003827-01.

References

1. M. Schena, *Microarray Analysis* (Wiley, 2003).
2. H. Zhu, M. Bilgin, R. Bangham, D. Hall, A. Casamayor, P. Bertone, Ning Lan, R. Jansen, S. Bidlingmaier, T. Moufek, T. Mitchell, P. Miller, R. A. Dean, M. Gerstein, and M. Scheider, "Global analysis of protein activities using proteome chips," Science **293,** 2101–2105 (2001).
3. G. MacBeath, "Protein microarrays and proteomics," Nat. Genet. **32,** 526–532 (2002).
4. T. Lindahl and R. D. Wood, "Quality control by DNA repair," Science **286,** 1897–1905 (1999).
5. B. P. Nelson, A. G. Frutos, J. M. Brockman, and R. M. Corn, "Near-infrared surface plasmon resonance measurements of ultrathin films. 1. Angle shift and SPR imaging experiments," Anal. Chem. **71,** 3928–2934 (1999).
6. J. S. Shumaker-Parry and C. T. Campbell, "Quantitative methods for spatially resolved adsorption/desorption measurements in real time by surface plasmon resonance microscopy," Anal. Chem. **76,** 907–917 (2004).
7. L. S. Jung, C. T. Campbell, T. M. Chinowsky, M. N. Mar, and S. S. Yee, "Quantitative interpretation of the response of surface plasmon resonance sensors to adsorbed films," Langmuir **14,** 5636–5648 (1998).
8. R. M. A. Azzam and N. M. Bashara, *Ellipsometry and Polarized Light* (Elsevier Science, 1987).
9. G. Jin, R. Jansson, and H. Arwin, "Imaging ellipsometry revisited: development for visualization of thin transparent layers on silicon substrates," Rev. Sci. Instrum. **67,** 2930–2936 (1996).
10. Z. H. Wang and G. Jin, "A label-free multi-sensing immunosensor based on imaging ellipsometry," Anal. Chem. **75,** 6119–6123 (2003).
11. J. P. Landry, J. P. Gregg, and X. D. Zhu, "Label-free detection of microarrays of biomolecules by oblique-incidence reflectivity difference microscopy," Opt. Lett. **29,** 581–583 (2004).
12. J. Piehler, A. Brecht, and G. Gauglitz, "Affinity detection of low molecular weight analytes," Anal. Chem. **68,** 139–143 (1996).
13. P. Thomas, E. Nabighian, M. C. Bartelt, C. Y. Fong, and X. D. Zhu, "An oblique-incidence optical reflectivity difference and LEED study of rare-gas growth on a lattice-mismatched metal substrate," Appl. Phys. A **79,** 131–137 (2004).
14. Y. Y. Fei, X. D. Zhu, L. F. Liu, H. B. Liu, Z. H. Chen, and G. Z. Yang, "Oscillations in oblique-incidence optical reflection from a growth surface during layer-by-layer epitaxy," Phys. Rev. B **69,** 233405 (2004).
15. W. Schwarzacher, J. Gray, and X. D. Zhu, "Oblique incidence reflectivity difference as an *in situ* probe of electrodeposition: Co on Au," Electrochem. Solid-State Lett. **6,** C73–C76 (2003).
16. X. D. Zhu, "Oblique-incidence optical reflectivity difference from a rough film of crystalline material," Phys. Rev. B **69,** 115407 (2004).
17. J. P. Landry, J. Gray, M. K. O'Toole, and X. D. Zhu, "Incidence-angle dependence of optical reflectivity difference from an ultrathin film on solid surface," Opt. Lett. **31,** 531–533 (2006).
18. B. Liedberg, C. Nylander, and I. Lundstrom, "Surface plasmon resonance for gas detection and biosensing," Sens. Actuators **4,** 299–304 (1983).
19. X. D. Zhu, "Comparison of two optical techniques for label-free detection of biomolecular microarrays on solids," Opt. Commun. **259,** 751–753 (2006).
20. W. A. Hendrickson, A. Paehler, J. L. Smith, Y. Satow, E. A. Merritt, and R. P. Phizackerley, "Crystal structure of core streptavidin determined from multiwavelength anomalous diffraction of synchrotron radiation," Proc. Natl. Acad. Sci. USA **86,** 2190–2194 (1989).
21. P. Weber, D. Ohlendorf, J. Wendoloski, and F. Salemme, "Structural origins of high-affinity biotin binding to streptavidin," Science **243,** 85–88 (1989).